



RESEARCH ARTICLE

Evaluating the Role of Amide Proton Transfer (APT)–Weighted Contrast, Optimized for Normalization and Region of Interest Selection, in Differentiation of Neoplastic and Infective Mass Lesions on 3T MRI

Ayan Debnath,¹ Rakesh Kumar Gupta,² Anup Singh^{1,3}

¹Centre for Biomedical Engineering, Indian Institute of Technology Delhi, Block II, Room No. 299, New Delhi, 110016, India

²Fortis Memorial Research Institute, Gurgaon, India

³Department of Biomedical Engineering, All India Institute of Medical Sciences, New Delhi, India

Abstract

Purpose: To evaluate the role of amide proton transfer–weighted (APT-w) magnetic resonance imaging (MRI) in differentiating neoplastic and infective mass lesions using different contrast normalizations, region of interest (ROI) selection, and histogram analysis.

Procedures: Retrospective study included 32 treatment-naive patients having intracranial mass lesions (ICMLs): low-grade glioma (LGG) = 14, high-grade glioma (HGG) = 10, and infective mass lesions = 8. APT-w MRI images were acquired along with conventional MRI images at 3 T. APT-w contrast, corrected for B₀-field inhomogeneity, was computed and optimized with respect to different types of normalizations. Different ROIs on lesion region were selected followed by ROI analysis and histogram analysis. Statistical analysis was performed using Shapiro-Wilk's test, *t* tests, ANOVA with Tukey's post hoc test, and receiver operation characteristic (ROC) analysis.

Results: ICMLs showed significantly ($p < 0.01$) higher APT-w contrast in lesion compared with contralateral side. There was a substantial overlap between mean APT-w contrast of neoplastic and infective mass lesions as well as among different groups of ICMLs irrespective of ROI selection and normalizations. APT-w contrast (using type 4 normalization: normalized with reference signal at negative offset frequency and APT-w contrast in normal-appearing white matter) reduced variability of APT-w contrast across different subjects, and overlap was less compared with other types of normalizations. There was a significant difference ($p < 0.05$) between neoplastic and infective mass lesions using *t* test for different histogram parameters of type 4 normalized APT-w contrast. ANOVA with post hoc showed significant difference ($p < 0.05$) for different histogram parameters of APT-w contrast (Type 4 normalization) between LGG and HGG, LGG, and infective mass lesion. Histogram parameters such as standard deviation, mean of top percentiles, and median provided improved differentiation between neoplastic and infective mass lesions compared with mean APT-w contrast. A greater number of

Electronic supplementary material The online version of this article (<https://doi.org/10.1007/s11307-019-01382-x>) contains supplementary material, which is available to authorized users.

Correspondence to: Anup Singh; e-mail: anupsm@iitd.ac.in

histogram parameters of type 4 normalized APT-w contrast corresponding to active lesion region can significantly differentiate between ICMLs than other types of normalizations and ROIs.

Conclusions: APT-w contrast using type 4 normalization and active lesion region (ROI-2) should be used for studying APT. APT-MRI should be combined with other MRI techniques to further improve the differential diagnosis of ICMLs.

Key words: Chemical exchange saturation transfer (CEST), Amide proton transfer-weighted, MRI, Neoplastic mass lesions, Infective mass lesions, Intracranial mass lesions

Introduction

Most of the pathological processes are initiated by abnormal changes in biomolecular environment at the cellular level. *In vivo* and non-invasive detection of these biomolecules is important for diagnosis and characterization of diseases. Due to low concentration of these labile molecules, *in vivo* detection of these molecules is not possible using conventional imaging [1]. Recently, chemical exchange saturation transfer (CEST) [2–6] has been proposed as a novel non-invasive magnetic resonance imaging (MRI) contrast mechanism for high-resolution mapping of molecular information in biological tissues. CEST contrast at an offset frequency of +3.5 ppm from water protons resonance, at low saturation RF power, has been reported [7] to be sensitive to amide protons of labile peptides and small proteins. This contrast is widely known as amide proton transfer (APT) contrast [7–9]. More specifically, this contrast has additional signal contributions from other multiple confounding molecules, and thus, appropriate nomenclature is amide proton transfer-weighted (APT-w) [10] contrast. APT-w MRI is sensitive to low concentration of biomolecules (endogenous cellular proteins and peptides) [11] and tissue physiochemical properties (pH and temperature) [8, 12].

Preliminary studies have shown the potential applications of APT-MRI in stroke [12, 13], central nervous system (CNS) lymphoma [14], and brain tumor grading [7, 15–20]. Recently, one group has investigated APT-w contrast on lymphoma and compared with high-grade tumor [14]. Infective mass lesions in the CNS such as tuberculoma (TB) and neurocysticercosis (NCC) are widely prevalent in developing countries and sometimes behave similar to neoplastic mass lesions on conventional MRI. However, till date, there are no studies available on APT-w imaging of infective mass lesions and its comparison with neoplastic mass lesions. Conventional MRI images like T₂-w, FLAIR, and post contrast T₁-w (PCT₁-w) reveal the location and the appearance of lesions but does not provide enough knowledge about lesion classification. Standard MRIs along with other MRIs *viz.* dynamic contrast-enhanced (DCE) MRI, diffusion MRI, and magnetization transfer contrast though provide useful information for detection of infective and neoplastic mass lesions; still, there are some challenges [21] in their differentiation. Therefore, potential of APT-

w imaging in differentiating intracranial mass lesions (ICMLs) needs to be investigated.

Most of the reported studies [13, 14, 16, 19–21] have used magnetization transfer ratio (MTR) or CEST asymmetry (CEST_{asym}) to compute APT-w contrast. The conventional method of asymmetry analysis uses M_0 (signal intensity without radiofrequency (RF) saturation) for normalization. Some studies have suggested normalization by negative offset frequency ($M_{\text{sat}(-3.5 \text{ ppm})}$ which is the signal intensity at -3.5 ppm upfield from water resonating frequency (4.7 ppm which is considered as 0 ppm)) for increasing dynamic range of contrast [22]. Few studies reported normalization by mean APT-w contrast using normal-appearing white matter (NAWM) [15, 19] region for improved analysis. NAWM are regions on white matter with no visible hyper-intensity on T₂-w, FLAIR, and PCT₁-w images. Previous studies have used different types of normalizations in isolation. However, effect of different normalizations on APT-w contrast in terms of differentiation of ICMLs needs to be evaluated. Region of interest (ROI) selection on lesion plays an important role; therefore, optimization for ROI selection also needs to be carried out in terms of APT-w contrast's ability in differentiating ICMLs. Moreover, histogram analysis provides more insight to gain more information about lesion and thus might improve the diagnosis and grading [23–25].

We hypothesize that optimum normalization, ROI selection, and histogram analysis of APT-w contrast can improve differentiation of ICMLs. The purpose of this study was to investigate the potential of APT-w contrast in differentiating infective and neoplastic mass lesions and to determine the optimal combination using different types of normalizations, ROI selection, and histogram parameters for more sensitive detection of tumor against infection.

Materials and Methods

Patient Recruitment

MRI data of 32 treatment-naive patients (24 males, 8 females; mean age 43 years; range 11–82 years) with ICMLs were included in this study. This retrospective study was approved by the institutional ethics committee, and informed consent was obtained from the patients.

MR Imaging Sequence and Protocols

All the MRI experiments were performed on 3T whole body Inginia MRI system (Philips Healthcare, The Netherlands) using a 15-channel head-neck coil for reception. MRI data included following images as a part of clinical protocol: T_1 -w and T_2 -w turbo spin echo (TSE), fluid-attenuated inversion recovery (FLAIR), and post contrast-enhanced T_1 -w (PCT₁-w) images. The following parameters were used for T_2 -w: echo train length (ETL) 16, repetition time (TR)/echo time (TE) 3500 ms/90 ms, field of view (FOV) 240×240 mm², matrix size 256×256 , slice thickness 6 mm, slices 12, flip angle 90°; T_1 -w: ETL 4, TR/TE 360 ms/10 ms, FOV 240×240 mm², matrix size 256×256 , slice thickness 6 mm, slices 12, flip angle 70°; DWI: ETL 61, TR/TE 4096 ms/112 ms, FOV 243×230 mm², matrix size 192×192 , slice thickness 5 mm, slices 27, flip angle 90°, $b=0$ and 1000; FLAIR: ETL 167, TR/TE 4700 ms/290 ms, FOV 247×247 mm², matrix size 288×288 , slice thickness 0.9 mm, slices 25, flip angle 90°, inversion recover (IR) time 1650 ms. For acquiring PCT₁-w images, 0.1 mmol/kg body weight of gadobenate dimeglumine (Gd-BOPTA) (MultiHance, Bracco) was administered with the help of power injector at rate of 3 ml/s followed by bolus injection of a 30 ml saline flush. PCT₁-w image was acquired after 2 min of contrast injection. The parameters for PCT₁-w images are ETL 55, TR/TE 700 ms/24 ms, FOV 250×250 mm², matrix size 560×560 , slice thickness 0.9 mm, slices 25, flip angle 90°.

The APT-w MRI images were also acquired before the administration of the contrast agent [26]. The pulse sequence [27, 28] used to acquire APT-w MRI comprised of three sections: four blocks of radiofrequency saturation preparation pulses (each block with root mean square B_1 (B_{1rms}) of 2 μ T and duration of 200 ms) each followed by a crusher gradient (saturation duration of 10 ms and amplitude of 10 mT/m), lipid suppression (flip angle 100° and duration of 17.6 ms) followed by a crusher gradient (saturation duration of 2 ms and amplitude of 22 mT/m) and readout. APT-w images were acquired for a single representative slice (2D acquisition), positioned at center of lesion, with 64 frequency points (± 0 to ± 1792 Hz with step size of 64 Hz and unsaturated image at 10,000 Hz). Other imaging parameters were ETL 42, TR/TE 3000 ms/5.54 ms, FOV 212×212 mm², matrix size 176×176 , and flip angle 90°. Fat suppression was achieved using SPIR. Total scan time for 2D APT-w images was 5.0 min. Water saturation shift referencing (WASSR) [29] data was also acquired for generating B_0 map, which is required for B_0 inhomogeneity correction of APT-w images. WASSR images were collected for the same slice with 26 frequency points (-192 to $+192$ Hz with a step size of 16 Hz) using saturation B_{1rms} of 0.5 μ T and duration of 200 ms.

Theory

Exchangeable solute protons of amide group were selectively saturated using RF irradiation. Due to exchange of protons, the saturation was transferred to bulk water and thus water signal reduced. For computing APT-w contrast, the present study used four types of normalizations:

Type 1. APT-w contrast when normalized with M_0 (APT _{M_0}):

$$APT_{M_0} = \frac{M_{\text{sat}(-3.5\text{ppm})} - M_{\text{sat}(+3.5\text{ppm})}}{M_0} \times 100 \quad (1)$$

where $M_{\text{sat}(+3.5 \text{ ppm})}$ and $M_{\text{sat}(-3.5 \text{ ppm})}$ are the signal intensities with downfield and upfield of water resonating frequency.

Type 2. APT-w contrast when normalized with $M_{\text{sat}(-3.5 \text{ ppm})}$ (APT_{Neg}):

$$APT_{\text{Neg}} = \frac{M_{\text{sat}(-3.5\text{ppm})} - M_{\text{sat}(+3.5\text{ppm})}}{M_{\text{sat}(-3.5\text{ppm})}} \times 100 \quad (2)$$

Type 3. APT-w contrast when normalized with M_0 and NAWM (APT _{M_0 -NAWM}):

$$APT_{M_0\text{-NAWM}} = APT_{M_0} - M_1 \quad (3)$$

where M_1 is the mean value of APT _{M_0} -w contrast in NAWM.

Type 4. APT-w contrast when normalized with $M_{\text{sat}(-3.5 \text{ ppm})}$ and NAWM (APT_{Neg-NAWM}):

$$APT_{\text{Neg-NAWM}} = APT_{\text{Neg}} - M_2 \quad (4)$$

where M_2 is the mean value of APT_{Neg}-w contrast in NAWM.

Usually, MTR asymmetry or CEST_{asym} analysis mitigates the effect of direct saturation (DS) and magnetization transfer (MT) with the assumption that DS and MT are symmetrical [30] around water resonating frequency. As such, for *in vivo* data, there is a small MT asymmetry effect, which confounds APT-w contrast. Along with this, relayed

nuclear Overhauser effect (rNOE) effect also contaminates APT-w contrast using asymmetry analysis.

Image Processing and Analysis

All the data processing was performed using in-house written programs in MATLAB R2014-R2017 (The MathWorks, Inc., MA, USA). The pre-processing steps included registration of APT-w, WASSR, T_2 -w, PCT_1 -w, and FLAIR images with T_1 -w images followed by automated de-scalping of APT-w images for background noise removal. The registration and de-scalping were carried out using SPM12 software. B_0 map was generated using WASSR methodology [29]. APT-w images at ± 3.5 ppm (± 448 Hz) were corrected for B_0 inhomogeneity using neighborhood frequency offset data (± 320 to ± 576 Hz with step size of 64 Hz). Finally, APT-w maps were computed using type 1, 2, 3, and 4 normalization approaches as described in the previous section. In this study, single slice APT-w images were processed and analyzed.

ROI Selection and Analysis

In-house developed semiautomatic lesion segmentation approach based upon seeded region growing algorithm [31] and morphological operations was used to segment out different parts of lesion. Firstly, hyper-intense region or contrast-enhancing region of PCT_1 -w image was segmented out using region growing algorithm, and this region corresponds to active lesion region (ROI-2). For non-enhancing lesions ($n=6$), ROI-2 was selected by experienced radiologist on T_2 -w image using polygon ROI selection in MATLAB R2017. Secondly, hyper-intense region on FLAIR image was segmented using same semiautomatic segmentation approach. Lastly, FLAIR hyper-intense mask was combined with contrast-enhancing mask (ROI-2) to obtain entire lesion region (ROI-1). Contralateral regions of ROI-1 and ROI-2 (cROI-1 and cROI-2) were generated automatically using in-house developed MATLAB code. In addition, NAWM and normal-appearing gray matter (NAGM) masks were also obtained using SPM-12 software with T_1 -w images. Entire lesion region (ROI-1) was excluded from NAWM and NAGM followed by morphological operation erosion (kernel size – 3×3) to obtain pure NAMW mask and NAGM mask and to remove contribution from partial volume effects.

Average APT-w contrast in NAWM was used to compute $APT_{M_0_NAWM}$ contrast using type 3 normalization and APT_{Neg_NAWM} contrast using type 4 normalization. Mean and standard deviation (SD) of APT-w contrast corresponding to different types of normalizations were computed from the abovementioned ROIs. APT-w contrast was reported in the study as mean \pm SD. Box and whisker plots were also generated to provide a graphical

representation of data distribution of APT-w contrast. Computed APT-w maps were color overlaid on anatomical images.

Histogram Analysis

Histogram analysis [23–25] of APT-w contrast using type 3 and type 4 normalizations corresponding to ROI-1 and ROI-2 was carried out. Apart from mean and SD, the following histogram parameters were calculated: (a) median; (b) mode; (c) kurtosis; (d) skewness; (e) entropy; (f) full width at half maximum (FWHM); (g) 10th, 25th, 50th, 75th, and 90th percentile (pr_10, pr_25, pr_50, pr_75, and pr_90); (h) mean of the values greater than 10th, 25th, 50th, 75th, and 90th percentile (mtop10, mtop25, mtop50, mtop75, mtop90); and (i) standard deviations of the values greater than 10th, 25th, 50th, 75th, and 90th percentile (sdtop10, sdtop25, sdtop50, sdtop75, sdtop90).

Statistical Analysis

Tests for normality were carried out for all the parameters of APT-w contrast extracted from both ROI-1 and ROI-2 using Shapiro-Wilk's test. This test was carried out for each group of ICMLs (low-grade glioma (LGG), high-grade glioma (HGG), and infective mass lesions) separately. After normality testing, mean, median, mode, and other histogram parameters of APT-w contrast were compared between neoplastic mass lesion and infective mass lesion using independent Student's t test with two tails. Histogram parameters of APT-w contrast were also compared among different groups of ICMLs (LGG, HGG, and infective mass lesions) using a one-way analysis of variance (ANOVA) with Tukey's honestly significant difference (HSD) post hoc test. While differentiating lesion from contralateral region, independent Student's t test was used. The difference was considered statistically significant if $p < 0.05$. Receiver operation characteristic (ROC) analysis was conducted to evaluate the diagnostic performance of the histogram parameters in differentiating neoplastic from infective mass lesion, as well as in differentiating ICMLs. Sensitivity, specificity, area under curve (AUC) with 95 % confidence interval (CI), accuracy, and cutoff were computed in ROC analysis. Statistical analysis was performed with a commercially available software package SPSS.v.15 (IBM SPSS Statistics, v. 15.0; Armonk, NY).

Results

Pathological Diagnosis

A total of 24 neoplastic mass lesions and 8 infective mass lesions were included in this study. Neoplastic mass lesion includes 14 LGG (pilocytic astrocytoma = 6, WHO grade I; ganglioglioma = 1, WHO grade I; astrocytoma = 5, WHO

grade II; oligodendroglioma=2, WHO grade II) and 10 HGG (anaplastic astrocytoma=4, WHO grade III; anaplastic oligoastrocytoma=1, WHO grade III; ganglioglioma=1, WHO grade III; glioblastoma (GBM)=4, WHO grade IV). Infective mass lesion includes eight patients (TB=3, tubercular abscess=1, aspergillus granuloma=1, NCC=3).

APT-W Contrast Measurement by Different Normalizations

Infective and neoplastic mass lesions in the current study showed significantly ($p < 0.01$) higher APT-w contrast compared with its contralateral side (Figs. 1 and 2). For all types of normalizations, APT-w contrast corresponding to ROI-1 and ROI-2 was significantly ($p < 0.01$) higher compared with cROI-1 and cROI-2, respectively. In general, it was found that mean APT-w contrast in NAWM regions is lower than APT-w contrast in NAGM for all types of normalizations (Fig. S1, see Electronic Supplementary Material (ESM)). Figure S1 shows that APT_{M0_NAWM} contrast (type 3 normalization) and APT_{Neg_NAWM} contrast (type 4 normalization) have higher dynamic range and smaller inter-quartile range than APT_{M0} contrast (type 1 normalization) and APT_{Neg} contrast (type 2 normalization). Figure S1c and d shows that median has been shifted to the center of box plots, which indicate symmetry in distribution of the data. Figure 1 shows necrotic region with hypointense APT-w contrast compared with active tumor. It shows that APT-w maps can clearly differentiate necrotic or cystic regions from active lesions. The APT-w maps show a difference in contrast between WM, GM, and intracranial lesions. Figure 2 shows that variability for NAWM and NAGM across different subjects was reduced in APT_{M0_NAWM} contrast (column 8) and APT_{Neg_NAWM} contrast (column 9), whereas variability for NAWM and NAGM tissues across different subjects was more in APT_{M0} contrast (column 6) and APT_{Neg} contrast (column 7). Figure S2 (see ESM) shows the selections of ROIs on a representative case of HGG.

The box and whisker plots in Fig. 3 show that there is a substantial overlap of mean APT-w contrast of neoplastic and infective mass lesions for all types of normalizations corresponding to ROI-1 and ROI-2. The mean APT_{M0} contrast (type 1 normalization) and APT_{Neg} contrast (type 2 normalization) for neoplastic mass lesions were 1.35 ± 0.98 % and 2.21 ± 1.69 % (for ROI-1) and 1.53 ± 1.16 % and 2.52 ± 1.98 % (for ROI-2), respectively. The mean APT_{M0} contrast (type 1 normalization) and APT_{Neg} contrast (type 2 normalization) for infective mass lesions were 1.31 ± 0.62 % and 2.35 ± 1.15 % (for ROI-1) and 1.71 ± 0.83 % and 3.09 ± 1.53 % (for ROI-2). This showed that mean APT-w contrast is higher in type 2 than type 1 normalization.

The box and whisker plots (Fig. 4) provide comparison of average APT-w contrast for different groups of ICMLs,

using type 1, 2, 3, and 4 normalizations, corresponding to ROI-1 and ROI-2. For all kinds of ROIs and normalizations, there is a substantial overlap among mean APT-w contrast of LGG, HGG, and infective mass lesions. The mean APT_{M0} contrast (type 1 normalization) is lower than APT_{Neg} contrast (type 2 normalization) for all ICMLs corresponding to ROI-1 and ROI-2. The mean APT-w contrast for HGG is higher than LGG for all types of normalizations and ROIs. The APT-w contrast corresponding to type 4 normalization and ROI-2 for LGG was 3.58 ± 0.65 and HGG was 5.14 ± 0.811 .

Statistical Analysis (Shapiro-Wilk's Test for Normality)

Normality test showed that the data sets considered in this study were normally distributed. A Shapiro-Wilk's test ($p > 0.05$) showed that mean APT_{Neg_NAWM} contrast (type 4 normalization) corresponding to ROI-2 was normally distributed for LGG [p value = 0.36, skewness = -0.18 (standard error (SE) = 0.59), kurtosis = -1.37 (SE = 1.15)], HGG [p value = 0.12, skewness = 0.91 (SE = 0.69), kurtosis = 0.83 (SE = 1.33)], and infection [p value = 0.79, skewness = 0.81 (SE = 0.75), kurtosis = 0.31 (SE = 1.48)]. Similarly, other histogram parameters also showed normal distributions for all types of normalized APT-w contrast.

Statistical Analysis (t Test)

Table 1 shows only those histogram parameters which can significantly differentiate ($p < 0.05$) between neoplastic and infective mass lesions using independent Student's t test. Mean of APT-w contrast for type 1, type 2, and type 3 normalizations showed insignificant difference between neoplastic and infective mass lesions for all ROIs. The mean APT_{Neg_NAWM} contrast (type 4 normalization) can significantly differentiate ($p < 0.05$) neoplastic from infective mass lesions for ROI-2 (Table 1) and not for ROI-1. While comparing histogram parameters of APT-w contrast corresponding to ROI-1 and ROI-2, a greater number of histogram parameters can significantly differentiate ($p < 0.05$) neoplastic from infective mass lesions corresponding to ROI-2 considering type 4 normalization (Table 1). Similar number of histogram parameters can significantly differentiate ($p < 0.05$) between neoplastic and infective mass lesions for ROI-1 and ROI-2 considering type 3 normalization. While comparing histogram parameters of APT-w contrast corresponding to type 3 and type 4 normalizations, a greater number of histogram parameters of type 4 than type 3 normalizations can significantly differentiate ($p < 0.05$) between neoplastic and infective mass lesions for both ROI-1 and ROI-2.

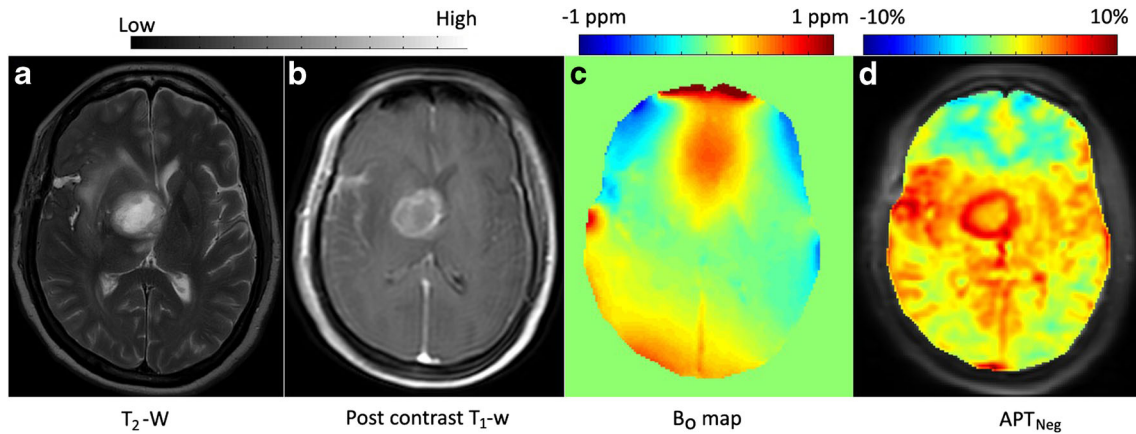


Fig. 1 A representative case of intracranial mass lesions (ICMLs). **a** T₂-weighted (w), **b** post contrast T₁-w image, **c** B₀ map, and **d** APT_{Neg} map. Active region of lesion shows hyper-intense APT-w contrast compared with contralateral region and other portions of the brain slice. Necrotic region of the lesion has lower APT-w contrast compared with active tumor.

Statistical Analysis (ANOVA with Post Hoc Test)

Table 2 demonstrates histogram parameters which can significantly differentiate ICMLs using one-way ANOVA test. Mean of APT-w contrast for type 1, type 2, and type 3 cannot significantly differentiate different group of ICMLs for both ROI-1 and ROI-2. Only mean of APT_{Neg_NAWM} contrast (type 4 normalization) corresponding to ROI-2 can significantly differentiate ($p < 0.05$) among different group of ICMLs. There were a greater number of histogram parameters for type 4 normalization corresponding to ROI-2 which provide significant difference ($p < 0.05$) among ICMLs. One-way ANOVA with Tukey’s HSD post hoc test showed a significant difference ($p < 0.05$) between LGG and infection for different histogram parameters of type 4

normalizations corresponding to ROI-2. The mode of type 4 normalization provided significant difference ($p < 0.05$) between LGG and HGG corresponding to ROI-2. The skewness of type 3 normalization can significantly differentiate ($p < 0.05$) HGG from infection corresponding to ROI-1. The mean, SD, median, mtop10, mtop25, mtop50, mtop75, and mtop90 of type 4 normalization provided significant difference ($p < 0.05$) between neoplastic and infective mass lesions corresponding to ROI-2.

ROC Analysis

The present study shows ROC analysis of those histogram parameters which provided significant difference in

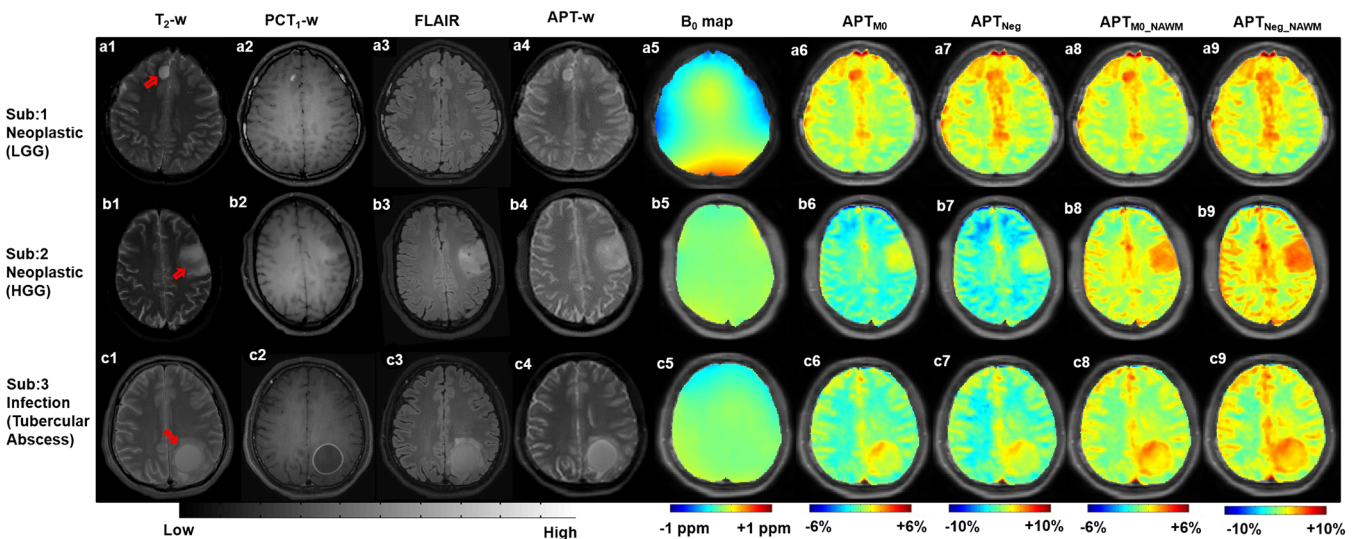


Fig. 2 Rows 1–3 show MRI images of representative neoplastic mass lesion (low-grade glioma (LGG) and high-grade glioma (HGG)) and infective mass lesion (tubercular abscess), respectively. Columns 1–9 contain T₂-weighted (w), post contrast T₁-w (PCT₁-w), FLAIR, APT-w images, B₀ map, APT_{M0}, APT_{Neg}, APT_{M0_NAWM}, and APT_{Neg_NAWM} maps, respectively. APT_{M0_NAWM} (type 3) and APT_{Neg_NAWM} (type 4) normalizations reduce the variability between NAWM and NAGM than APT_{M0} (type 1) and APT_{Neg} (type 2) normalizations. Red arrows point to lesion region. NAWM normal-appearing white matter, NAGM normal-appearing gray matter.

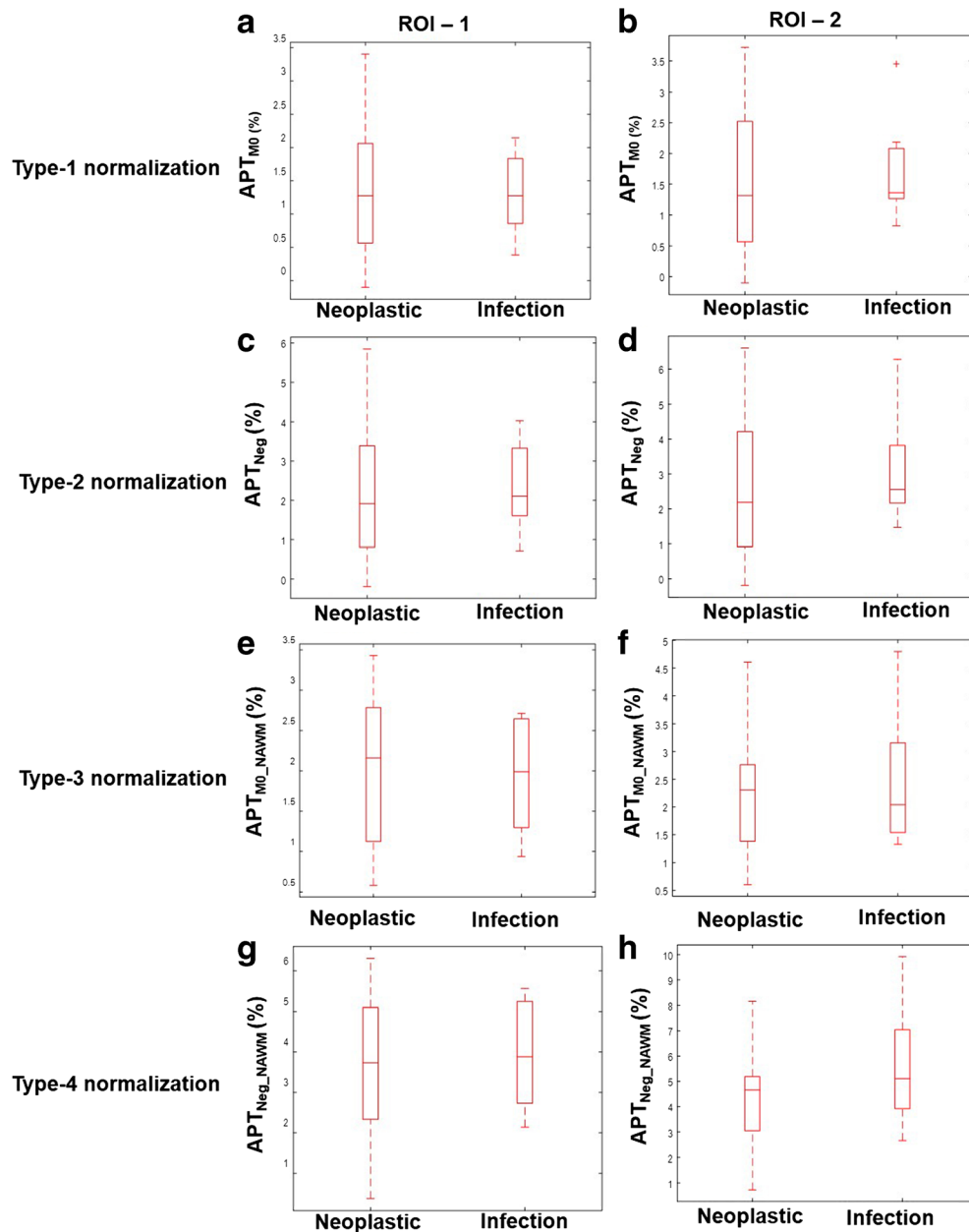


Fig. 3 Box and whisker plots show quantitative comparison of neoplastic and infective mass lesions for all types of APT-w contrast normalizations corresponding to two ROIs. ROI-1 represents entire lesion, and ROI-2 is active lesion region. Type 1, type 2, type 3, and type 4 normalizations represent APT_{MO} , APT_{Neg} , APT_{MO_NAWM} , and APT_{Neg_NAWM} contrast, respectively. Different range of scale was used for different normalizations to obtain better representation and visualization of individual plots. APT-w amide proton transfer weighted, ROI region of interest.

distinguishing neoplastic from infective mass lesions as well as in between different group of ICMLs. Table 3 shows ROC analysis of different histogram parameters for type 4 normalization corresponding to ROI-2 to distinguish neoplastic from infective mass lesions. Figure 5 demonstrates ROC analysis of mean of type 4 (Fig. 5a) normalized APT-w contrast considering ROI-2 to differentiate between neoplastic and infective mass lesions. In the discrimination between neoplastic and infective mass lesions using mean of type 4 normalization corresponding to ROI-2, a sensitivity and a specificity of 50 % and 80 %, respectively, were

observed with accuracy of 72 % and AUC was 65 %, when a cutoff value of 5.3 % was applied. Figure 5b and Table 4 show ROC analysis of APT_{Neg_NAWM} contrast (type 4 normalization) corresponding to ROI-2 in distinguishing LGG from infective mass lesions. ROC analysis provided a sensitivity of 62.5 %, a specificity of 71.43 %, AUC of 73.21 %, accuracy of 68.18 %, and cutoff value 4.77 % in distinguishing between LGG and infective mass lesions.

All the percentile parameters (pr_{10} , pr_{25} , pr_{50} , pr_{75} , and pr_{90}) and mean of top percentiles ($mtop_{10}$, $mtop_{25}$, $mtop_{50}$, $mtop_{75}$, $mtop_{90}$) provided significant difference

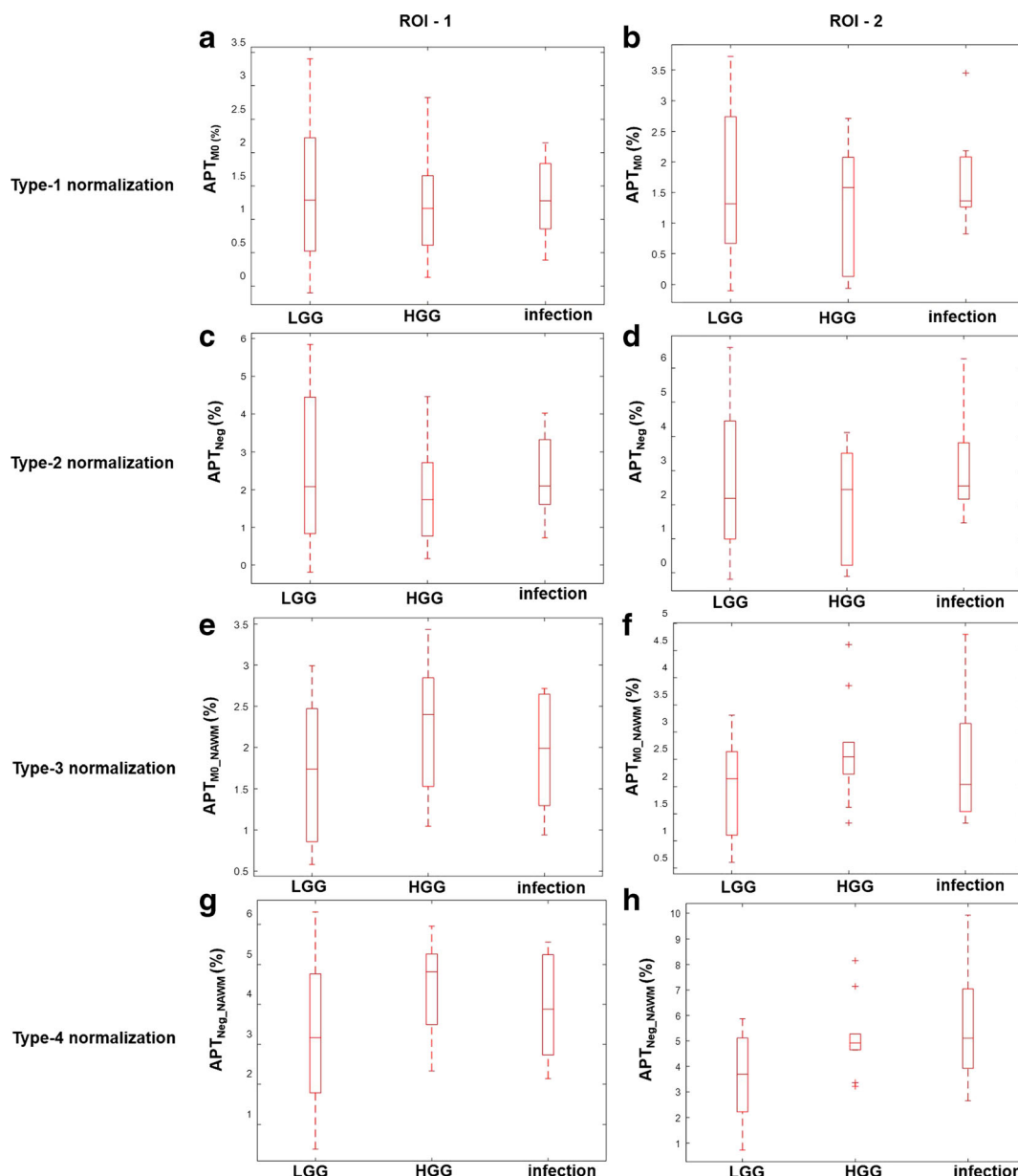


Fig. 4 Box and whisker plots show quantitative comparison of different types of APT-w contrast normalizations among different groups of ICMLs for two ROIs. ROI-1 represents entire lesion, and ROI-2 is active lesion region. Type 1, type 2, type 3, and type 4 normalizations represent APT_{M0} , APT_{Neg} , APT_{M0_NAWM} , and APT_{Neg_NAWM} contrast, respectively. Different range of scale was used for different normalizations to obtain better representation and visualization of individual plots. APT-w amide proton transfer weighted, ROI region of interest, LGG low-grade glioma, HGG high-grade glioma.

($p < 0.05$) simultaneously. Therefore, only mtop10, mtop25, mtop50, mtop75, and mtop90 were mentioned in tables. The mean of values greater than top percentiles of type 3 and type 4 normalized APT-w contrast was higher in HGG than LGG considering ROI-1 and ROI-2. The SD of APT_{M0_NAWM} contrast (type 3 normalization) corresponding to ROI-2 was 0.42 and 0.55 in LGG and HGG, respectively, whereas SD of APT_{Neg_NAWM} contrast (type 4 normalization) corresponding to ROI-2 was 0.65 and 0.81 in LGG and HGG, respectively. It showed that SD of APT-w contrast was higher in HGG than LGG. FWHM of APT_{Neg_NAWM} contrast (type 4 normalization)

corresponding to ROI-2 were 0.59 and 0.96 for LGG and HGG, respectively. Tables 1, 2, 3, and 4 show histogram parameters in details.

Discussion

The present study demonstrates that APT-w contrast were significantly higher in ICMLs compared with the contralateral region, NAWM, and NAGM. Similar findings were reported in previous studies [16] on tumor tissues, which mentioned increase in APT-w contrast in lesion regions compared with normal tissue regions. This occurs due to

Table 1. Histogram parameters of type 3 and type 4 normalizations, corresponding to ROI-1 and ROI-2, which provide significance difference ($p < 0.05$), using t test, between neoplastic and infective mass lesions

	ROI-1		ROI-2	
	Histogram parameters	p value (t test)	Histogram parameters	p value (t test)
type 3 normalization	Skewness	0.03	Kurtosis	0.04
	sdtop50	0.03	Entropy	0.05
	sdtop75	0.03	FWHM	0.03
type 4 normalization	Skewness	0.03	Mean	0.05
	sdtop10	0.05	SD	0.02
	sdtop25	0.03	Kurtosis	0.04
	sdtop50	0.01	mtop50	0.05
	sdtop90	0.01	mtop75	0.04
			mtop90	0.04
			sdtop10	0.03
		sdtop25	0.01	

increased cellular protein and peptide contents in lesion regions. The smaller inter-quartile range in the box plots of type 3 and type 4 normalizations resulted in reducing the inter-subject variability of APT-w contrast in both WM and GM tissues. Results of the current study agree with those reported by Wen et al. [11] and other studies [32], demonstrating that the average APT-w contrast was significantly lower in the necrotic or cystic region compared with healthy contralateral region. This can be linked with biological characteristics of the lesion. Higher endogenous mobile protein and peptide concentration is found in active lesion than necrotic regions.

One of the main purposes of the current study was to evaluate the role of different APT normalizations for differentiating neoplastic and infective mass lesions as well as ICMLs. In the present study, it was observed that mean APT-w contrast, using all types of normalizations, was higher in HGG compared with LGG, but statistical difference was non-significant ($p > 0.05$). Our results are in line with previous studies [15, 33] which observed a similar

trend due to higher concentration of proteins and peptides in HGG compared with LGG. HGG has higher microvasculature than LGG which reflects in higher APT-w contrast in HGG compared with LGG. Previously reported study [19] has also shown that there was a non-significant difference between LGG and HGG. Recent study by Togao et al. [15] showed that there was no strict threshold value in grading of tumors; APT-w contrast was around 2 in grade II, 3 in grade III, and 4 in grade IV. The current study could not find significant difference among ICMLs (like LGG and infection) if we consider type 1 and type 2 normalizations, but there was significant difference among them considering type 3 and type 4 normalizations for the same ROI-2. This might be due to the internal normalization, which reduces variability among different subjects and hence improves differentiation. Type 2 normalization increases the dynamic range of CEST_{asym} contrast compared with type 1 normalization [21]. Thus, mean APT-w contrast is always higher in type 2 than type 1 normalizations. One point that is noteworthy to mention is that

Table 2. Histogram parameters of type 3 and type 4 normalizations, corresponding to ROI-1 and ROI-2, which provide significance difference ($p < 0.05$), using one-way ANOVA, between different groups of intracranial mass lesions

	ROI-1			ROI-2		
	Histogram parameters	p value (ANOVA)	p value (post hoc)	Histogram parameters	p value (ANOVA)	p value (post hoc)
type 3 normalization	Skewness	0.06	0.05 ^c	mtop50	0.04	0.06 ^b
	sdtop10	0.05	0.05 ^b	mtop75	0.03	0.05 ^b
	sdtop50	0.05	0.04 ^b	mtop90	0.03	0.05 ^b
	sdtop75	0.06	0.05 ^b			
type 4 normalization	sdtop25	0.04	0.03 ^b	Mean	0.03	0.04 ^b
	sdtop50	0.02	0.01 ^b	SD	0.05	0.04 ^b
	sdtop75	0.02	0.01 ^b	Median	0.03	0.05 ^b
				Mode	0.02	0.04 ^a
				mtop10	0.03	0.04 ^b
				mtop25	0.02	0.03 ^b
				mtop50	0.01	0.02 ^b
				mtop75	0.01	0.01 ^b
				mtop90	0.01	0.01 ^b
				sdtop25	0.03	0.03 ^b

^a $p < 0.05$ between low-grade glioma (LGG) and high-grade glioma (HGG)^b $p < 0.05$ between low-grade glioma (LGG) and infection^c $p < 0.05$ between high-grade glioma (HGG) and infection

Table 3. ROC analysis of type 4 normalized APT-w contrast corresponding to ROI-2 for differentiating neoplastic from infective mass lesions

HP	<i>p</i> value	Sensitivity (%)	Specificity (%)	AUC (lb, ub) (%)	Cutoff (%)	Accuracy (%)
Mean	0.05	50	80	65 (42, 88)	5.3	72
SD	0.02	62.5	58.3	67 (42, 92)	0.69	84.37
Kurtosis	0.04	25	67	27 (4, 48)	2.87	56.25
mtop50	0.05	75	58.3	68 (47, 90)	5.29	62.5
mtop75	0.04	75	62.5	70 (47, 91)	5.81	65.62
mtop90	0.04	75	58.3	68 (46, 91)	5.98	62.5
sdtop10	0.03	62.5	70.8	66 (41, 91)	0.71	68.75
sdtop25	0.01	62.5	75	68.23 (42, 95)	0.64	71.88

AUC area under curve, *lb* lower bound with 95 % confidence interval, *ub* upper bound with 95 % confidence interval, *HP* histogram parameter

contralateral ROIs were not used for any kind of normalizations used in this study because contralateral ROIs may involve WM and GM with significantly different contrast variability. APT-w contrast showed less variability in NAWM; therefore, average value in this tissue was used for normalization. Type 3 and type 4 normalizations used NAWM reference region, which decreased variability among subjects and hence improved the differentiation of ICMLs [33]. APT-w contrast which were normalized with NAWM, *i.e.*, APT_{MO_NAWM} contrast (type 3 normalization) and APT_{Neg_NAWM} contrast (type 4 normalization), can be used as a biomarkers for differentiation between neoplastic and infective mass lesions [34]. In the current study, APT-w contrast in NAWM were negative; therefore, type 3 and type 4 normalizations resulted in an increase in values compared with type 1 and type 2 normalizations. Different type of normalizations provides a comprehensive view and better degree of freedom to compute APT-w contrast, which improves differentiation of ICMLs.

Placement of ROIs plays a crucial role in differentiating ICMLs. Manual selection of ROIs [35, 36] is subjective and can lead to substantial variation in measurements, hampering

the reliability of histogram and statistical analysis. Thus, in the current study, a semiautomatic approach was adopted for ROI selection to reduce subjectivity or bias. The combination of seeded region growing algorithm followed by morphological operations has been implemented in the current study for semiautomated ROI selection process. NAWM and NAGM masks that were generated using SPM-12 software might be erroneous, particularly for images having large size lesions. Thus, to obtain pure NAWM and pure NAGM, entire lesion mask regions was subtracted from NAWM and NAGM masks.

Histogram analysis of APT-w contrast has been used to grade cerebral tumors [23–25]. We considered histogram analysis of type 3 and type 4 normalized APT-w contrast because normalizations with NAWM decrease the variabilities between subjects. Histogram analysis has been carried on both ROI-1 and ROI-2 because ROI-1 takes care of the entire lesion (active tumor along with necrosis/cystic and edema) whereas ROI-2 is only concerned about active tumor region. There were six tumor patients ($n = 6$), among the whole patient data set used in this current study, with the presence of necrotic region. The APT-w contrast

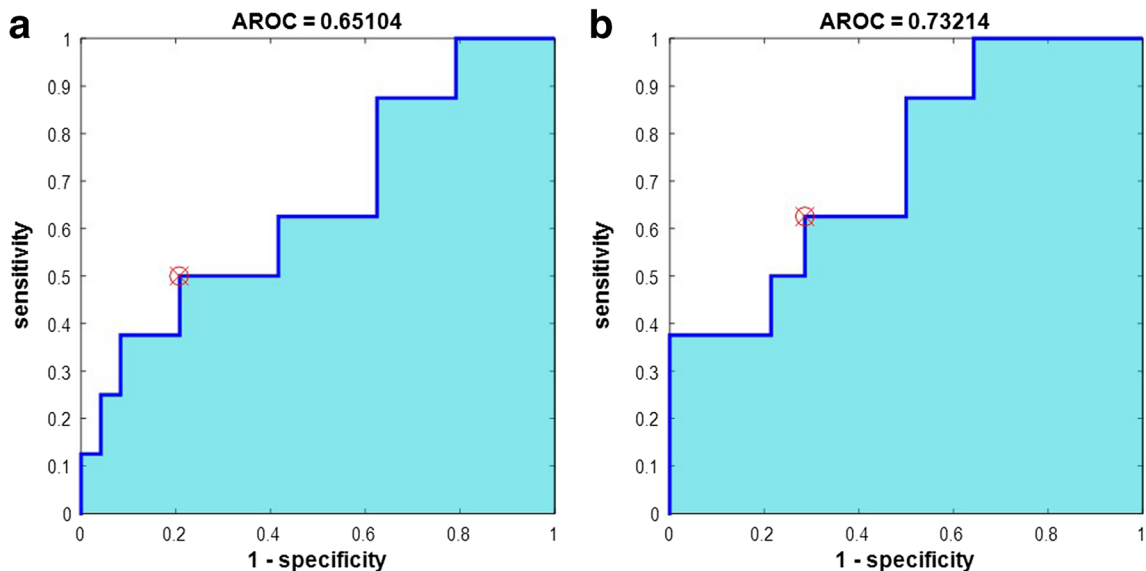


Fig. 5 ROC analysis of mean APT_{Neg_NAWM} -w contrast (type 4 normalizations) corresponding to ROI-2 for differentiation between **a** neoplastic and infective mass lesion and between **b** low-grade glioma and infective mass lesion. AROC area under curve for ROC plot.

Table 4. ROC analysis of type 4 normalized APT-w contrast corresponding to ROI-2 to differentiate low-grade glioma (LGG) and infective mass lesions

HP	<i>p</i> value (post hoc)	Sensitivity (%)	Specificity (%)	AUC (lb, ub) (%)	Cutoff (%)	Accuracy (%)
Mean	0.04	62.5	71.43	73.21 (51, 95)	4.77	68.18
SD	0.04	87.5	50	71.4 (46, 96)	0.58	81.81
Median	0.05	62.5	71.43	74.1 (53, 95)	4.68	68.18
mtop10	0.04	62.5	71.43	73.2 (51, 95)	4.39	68.18
mtop25	0.03	87.5	57.14	75 (54, 96)	4.46	68.18
mtop50	0.02	75	71.43	76.8 (56, 97)	5.21	72.72
mtop75	0.01	75	71.43	75.9 (55, 96)	5.60	72.72
mtop90	0.01	75	71.43	75 (53, 96)	5.78	72.72
sdtop25	0.03	62.5	78.57	71.4 (45, 97)	0.64	72.72

AUC area under curve, *lb* lower bound with 95 % confidence interval, *ub* upper bound with 95 % confidence interval, *HP* histogram parameter

corresponding to the necrotic region for all types of normalizations was slightly lower than active tumor region. The APT_{Neg_NAWM} contrast (type 4 normalization) was 3.51 ± 2.1 % corresponding to the necrotic region of $n = 6$ patients, whereas APT_{Neg_NAWM} contrast (type 4 normalization) was 4.6 ± 1.61 % in active tumor region corresponding to those $n = 6$ patients. Since APT-w values in necrotic tissue were slightly different than rest of tumor tissue and we had only six tumor patients, we did not exclude necrotic region from tumor during statistical analysis. In the future, for a large number of data set having necrotic region, separate ROI analysis can be carried out for necrotic and rest of tumor tissue. Independent Student's *t* test and one-way ANOVA results showed that a greater number of histogram parameters of type 4 normalization can differentiate neoplastic from infective mass lesions as well as among different groups of ICMLs than type 3 normalizations. This shows that type 4 normalization is better than type 1, 2, and 3 normalizations. Moreover, more histogram parameters corresponding to ROI-2 can differentiate neoplastic from infective mass lesions as well as among different categories of ICMLs than ROI-1. This shows that ROI analysis is better in ROI-2 than ROI-1. Histogram parameters *viz.* standard deviation, median, and mean of top percentiles provided improved differentiation between neoplastic and infective mass lesions compared with mean APT-w contrast. Histogram parameters like mean, SD, median, mode, mtop10, mtop25, mtop50, mtop75, and mtop90 are lower in LGG than HGG indicating higher severity in HGG. Histogram profile for HGG patients has been shifted towards right than histogram profile for LGG patients due to a higher mode. The current work studies the distribution of histogram profile of APT-w contrast, and it showed that neoplastic mass lesion has negative skewness while infective mass lesion has positive skewness. The sample data set for each group of ICMLs was little skewed and kurtotic, but it followed a normal distribution. FWHM of HGG is more than LGG, which also indicates that APT-w contrast of HGG is more diverged or heterogeneous. Thus, we assessed the usefulness of different histogram parameters and normalizations in predicting and differentiating ICMLs.

Previous studies [7] showed that APT-w MRI provides additional information about tumors than conventional

MRIs. The present study also reveals that there are some key advantages of APT-w MRI over conventional MRIs. Firstly, sometimes, PCT_1 -w images fail to enhance the lesion region whereas APT map clearly shows well-defined region of hyper-intensity (higher APT-w contrast) in the lesion region [10]. Secondly, T_2 -w images can detect lesions, but differentiation between active tumor region and necrotic or cystic region is difficult, whereas APT-w MRI can clearly differentiate necrotic region from active tumor region [32].

The current study uses asymmetry analysis based on various normalization techniques for computing APT-w contrast which has confounding effects from MT and rNOE. Recently, alternative *z*-spectra fitting-based approaches [37–39] are being developed for separating these effects, particularly at ultra-high fields. Recently, relaxation-compensated APT effects [40] are being analyzed to mitigate these confounding effects. CEST and rNOE peaks are quite broad at 3 T; therefore, further studies are required for robust *z*-spectra fitting.

There exist some limitations to the current study. Firstly, the number of patients, in each category of ICMLs, was small. Secondly, in this study, APT-w contrast was only corrected for B_0 inhomogeneity. Due to time constraint at clinical scanner, B_1 inhomogeneity correction was not performed. As such, B_1 -field inhomogeneity in brain at 3 T are quite small (~ 10 %) and should not affect the results of APT-w MRI substantially. Thirdly, in the current study, APT-w MRI data of a single representative slice was used. Three-dimensional [1] APT-w imaging might improve the coverage of lesion, providing more information and better signal-to-noise ratio (SNR).

Conclusion

The present study showed that APT-w contrast using type 4 normalization and appropriate histogram parameters corresponding to ROI-2 provided better differentiation between neoplastic and infective mass lesions as well as among different group of ICMLs. Thus, APT_{Neg_NAWM} (type 4 normalization) and active lesion region (ROI-2) should be used for studying APT-w MRI. APT-w MRI can be a promising tool in clinical settings for differentiating

infective and neoplastic mass lesions as well as ICMLs in combination with other MRI techniques.

Acknowledgments. The authors acknowledge Philips India Limited for technical support in MRI data acquisition. The authors thank Dr. Jinyuan Zhou, Dr. Peter C.M. Van Zijl, and Dr. Indrajit Saha for APT sequence and Dr. Mamta Gupta for editing manuscript. The authors also thank Dr. Sunita Ahlawat and Dr. Rana Patir for pathological information.

Funding Information. This work was supported by MATRICS scheme, Science and Engineering Research Board, Department of Science and Technology (SERB-DST) grant number MTR_2017_001021 for overall study and National Institutes of Health (NIH) grants P41 EB015909 for APT pulse sequence.

Compliance with Ethical Standards

Conflict of Interest

The authors declare that they have no conflict of interest.

References

- Zhao X, Wen Z, Zhang G, Huang F, Lu S, Wang X, Hu S, Chen M, Zhou J (2013) Three-dimensional turbo-spin-echo amide proton transfer MR imaging at 3-tesla and its application to high-grade human brain tumors. *Mol Imaging Biol* 15:114–122
- Sherry AD, Woods M (2009) Chemical exchange saturation transfer contrast agents for magnetic resonance imaging. *Annu Rev Biomed Eng* 10:391–411
- Vinogradov E, Sherry AD, Lenkinski RE (2013) CEST: from basic principles to applications, challenges and opportunities. *J Magn Reson* 229:155–172
- Liu G, Song X, Chan K W Y, McMahon MT (2013) Nuts and bolts of chemical exchange saturation transfer MRI. *NMR Biomed* 26:810–828
- Ward KM, Aletas AH, Balaban RS (2000) A new class of contrast agents for MRI based on proton chemical exchange dependent saturation transfer (CEST). *J Magn Reson* 143:79–87
- Van Zijl PCM, Yadav NN (2012) Chemical exchange saturation transfer (CEST): what is in a name and what isn't? *Magn Reson Med* 65:927–948
- Zhou J, Lal B, Wilson DA, Lartera J, van Zijl PCM (2003) Amide proton transfer (APT) contrast for imaging of brain tumors. *Magn Reson Med* 50:1120–1126
- Zhou J, Payen JF, Wilson DA et al (2003) Using the amide proton signals of intracellular proteins and peptides to detect pH effects in MRI. *Nat Med* 9:1085–1090
- Zhou J, Yan K, Zhu H (2008) A simple model for understanding the origin of the amide proton transfer MRI signal in tissue. *Magn Reson Med* 45:788–802
- Zhou J, Heo H, Knutsson L, Van Zijl PCM, Jiang S (2019) APT-weighted MRI: techniques, current neuro applications, and challenging issues. *J Magn Reson Imaging*: <https://doi.org/10.1002/jmri.26645>
- Wen Z, Hu S, Huang F, Wang X, Guo L, Quan X, Wang S, Zhou J (2010) MR imaging of high-grade brain tumors using endogenous protein and peptide-based contrast. *NeuroImage* 51:616–622
- Sun PZ, Cheung J, Wang E, Lo E (2011) Association between pH-weighted endogenous amide proton chemical exchange saturation transfer MRI and tissue lactic acidosis during acute ischemic stroke. *J Cereb Blood Flow Metab* 31:1743–1750
- Sun PZ, Murata Y, Lu J, Wang X, Lo EH, Sorensen AG (2008) Relaxation-compensated fast multislice amide proton transfer (APT) imaging of acute ischemic stroke. *Magn Reson Med* 59:1175–1182
- Jiang S, Yu H, Wang X, Lu S, Li Y, Feng L, Zhang Y, Heo HY, Lee DH, Zhou J, Wen Z (2016) Molecular MRI differentiation between primary central nervous system lymphomas and high-grade gliomas using endogenous protein-based amide proton transfer MR imaging at 3 tesla. *J Eur Radiol* 26:64–71
- Togao O, Yoshiura T, Keupp J, Hiwatashi A, Yamashita K, Kikuchi K, Suzuki Y, Suzuki SO, Iwaki T, Hata N, Mizoguchi M, Yoshimoto K, Sagiya K, Takahashi M, Honda H (2014) Amide proton transfer imaging of adult diffuse gliomas: correlation with histopathological grades. *Neuro-Oncology* 16:441–448
- Jones CK, Schlosser MJ, Van Zijl PCM et al (2006) Amide proton transfer imaging of human brain tumors at 3T. *Magn Reson Med* 56:585–592
- Debnath A, Sahoo P, Gupta P, Gupta RK, Singh A (2016) APT MRI of intracranial mass lesions at 3T and comparison with perfusion parameters. *Proceedings of International Society for Magnetic Resonance in Medicine (ISMRM): 24th Annual Meeting & Exhibition, May 7-13, Singapore, program number 3712*
- Togao O, Hiwatashi A, Yamashita K, Kikuchi K, Keupp J, Yoshimoto K, Kuga D, Yoneyama M, Suzuki SO, Iwaki T, Takahashi M, Iihara K, Honda H (2017) Grading diffuse gliomas without intense contrast enhancement by amide proton transfer MR imaging: comparisons with diffusion and perfusion-weighted imaging. *Eur Radiol* 27:578–588
- Sakata A, Okada T, Yamamoto A, Kanagaki M, Fushimi Y, Okada T, Dodo T, Arakawa Y, Schmitt B, Miyamoto S, Togashi K (2015) Grading glial tumors with amide proton transfer MR imaging: different analytical approaches. *J Neuro-Oncol* 122:339–348
- Bai Y, Lin Y, Zhang W et al (2015) Noninvasive amide proton transfer magnetic resonance imaging in evaluating the grading and cellularity of gliomas. *Oncotarget* 8:5834–5842
- Law M, Yang S, Wang H, Babb JS, Johnson G, Cha S, Knopp EA, Zagzag D (2003) Glioma grading: sensitivity, specificity, and predictive values of perfusion MR imaging and proton MR spectroscopic imaging compared with conventional MR imaging. *Am J Neuroradiol* 24:1989–1998
- Singh A, Cai K, Haris M, Hariharan H, Reddy R (2013) On B 1 inhomogeneity correction of in vivo human brain glutamate chemical exchange saturation transfer contrast at 7T. *Magn Reson Med* 69:818–824
- Kang Y, Choi SH, Kim KG (2011) Gliomas: histogram analysis of apparent diffusion coefficient maps with standard- or high- b-value diffusion-weighted MR imaging—correlation with tumor grade. *Neuroradiology* 261:882–890
- Law M, Young R, Babb J, Pollack E, Johnson G (2007) Histogram analysis versus region of interest analysis of dynamic susceptibility contrast perfusion MR imaging data in the grading of cerebral gliomas. *Am J Neuroradiol* 28:761–766
- Just N (2014) Improving tumour heterogeneity MRI assessment with histograms. *Br J Cancer* 111:2205–2213
- Tee YK, Donahue MJ, Harston GWJ et al (2013) Quantification of amide proton transfer effect pre- and post-gadolinium contrast agent administration. *J Magn Reson Imaging* 40:832–838
- Zhu H, Jones CK, Van Zijl PCM et al (2010) Fast 3D chemical exchange saturation transfer (CEST) imaging of the human brain. *Magn Reson Med* 64:638–644
- Zhou J, Zhu H, Lim M, Blair L, Quinones-Hinojosa A, Messina SA, Eberhart CG, Pomper MG, Lartera J, Barker PB, van Zijl PCM, Blakeley JO (2013) Three-dimensional amide proton transfer MR imaging of gliomas: initial experience and comparison with gadolinium enhancement. *J Magn Reson Imaging* 38:1119–1128
- Kim M, Gillen J, Landman BA, Zhou J, van Zijl PCM (2009) Water saturation shift referencing (WASSR) for chemical exchange saturation transfer (CEST) experiments. *Magn Reson Med* 61:1441–1450
- Zaiss M, Schmitt B, Bachert P (2011) Quantitative separation of CEST effect from magnetization transfer and spillover effects by Lorentzian-line-fit analysis of z-spectra. *J Magn Reson* 211:149–155
- Mehnert A, Jackway P (1997) An improved seeded region growing algorithm. *Pattern Recogn Lett* 18:1065–1071
- Zhou J, Tryggstad E, Wen Z, Lal B, Zhou T, Grossman R, Wang S, Yan K, Fu DX, Ford E, Tyler B, Blakeley J, Lartera J, van Zijl PCM (2011) Differentiation between glioma and radiation necrosis using molecular magnetic resonance imaging of endogenous proteins and peptides. *Nat Med* 17:130–134
- Park JE, Kim HS, Park KJ, Kim SJ, Kim JH, Smith SA (2016) Pre and posttreatment glioma: comparison of amide proton transfer imaging with MR spectroscopy for biomarkers of tumor proliferation. *Radiology* 278:514–523
- Debnath A, Gupta RK, Singh A (2019) To evaluate the role of APT-w contrast, optimized for normalization and ROIs selection, in differentiating infective and neo-plastic mass lesions. *Proceedings of International Society for Magnetic Resonance in Medicine (ISMRM):*

- 27th Annual Meeting & Exhibition, April 11-16, Canada, program number 4347
35. Jiang S, Zou T, Eberhart CG, Villalobos MAV, Heo HY, Zhang Y, Wang Y, Wang X, Yu H, du Y, van Zijl PCM, Wen Z, Zhou J (2017) Predicting IDH mutation status in grade II gliomas using amide proton transfer-weighted (APT_w) MRI. *Mag Reson Med* 78:1100–1109
 36. Yu H, Wen X, Wu P et al (2019) Can amide proton transfer-weighted imaging differentiate tumor grade and predict Ki-67 proliferation status of meningioma? *Eur Radiol* 18:1–9
 37. Cai K, Singh A, Popatni H et al (2015) CEST signal at 2ppm (CEST@2ppm) from Z-spectral fitting correlates with creatine distribution in brain tumor. *NMR Biomed* 28:1–8
 38. Debnath A, Singh A (2017) Lorentzian probabilistic sum based Z-spectrum fitting approach for computing CEST and NOE contrast and its comparison with lorentzian sum and asymmetry analysis. *Proceedings of International Society for Magnetic Resonance in Medicine (ISMRM): 25th Annual Meeting & Exhibition, April 22-27, Hawaii, program number 1975*
 39. Zaiss M, Xu LZ, Goerke S et al (2014) Inverse Z-spectrum analysis for spillover, MT and T1-corrected steady-state pulsed CEST-MRI-application to pH-weighted MRI of acute stroke. *NMR Biomed* 27:240–252
 40. Goerke S, Soehngen Y, Deshmane A et al (2019) Relaxation-compensated APT and rNOE CEST-MRI of human brain tumors at 3T. *Magn Reson Med* 00:1–11

Publisher's Note. Springer Nature remains neutral with regard to jurisdictional claims in published maps and institutional affiliations.